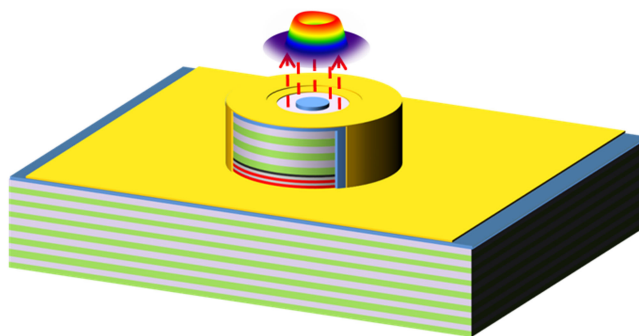


# Tailored Transverse Mode Vertical-Cavity Surface-Emitting Laser: Hollow Laser Beam Emission through Circle Aperture


Volume 12, Number 4, August 2020

Yinli Zhou  
Xing Zhang  
Jianwei Zhang  
Youwen Huang  
Yugang Zeng  
Jinjiang Cui  
Yun Liu  
Yongqiang Ning  
Lijun Wang



DOI: 10.1109/JPHOT.2020.3003927

# Tailored Transverse Mode Vertical-Cavity Surface-Emitting Laser: Hollow Laser Beam Emission through Circle Aperture

Yinli Zhou <sup>1</sup>, Xing Zhang,<sup>1,\*</sup> Jianwei Zhang,<sup>1</sup> Youwen Huang,<sup>1</sup>  
Yugang Zeng,<sup>1</sup> Jinjiang Cui,<sup>2,3</sup> Yun Liu,<sup>1</sup> Yongqiang Ning,<sup>1</sup>  
and Lijun Wang<sup>1</sup>

<sup>1</sup>State Key Laboratory of Luminescence and Application, Changchun Institute of Optics, Fine Mechanics and Physics, Chinese Academy of Sciences, Changchun 130033, China

<sup>2</sup>Suzhou Institute of Biomedical Engineering and Technology, Chinese Academy of Sciences, Suzhou 215163, China

<sup>3</sup>Jinan Guoke Medical Science & Technology Development Co., Ltd, Jinan 250000, China

DOI:10.1109/JPHOT.2020.3003927

This work is licensed under a Creative Commons Attribution 4.0 License. For more information, see <https://creativecommons.org/licenses/by/4.0/>

Manuscript received May 7, 2020; revised June 15, 2020; accepted June 17, 2020. Date of publication June 22, 2020; date of current version July 14, 2020. This work was supported in part by the National Key Research and Development Program under Grant 2018YFB2002400, in part by the National Natural Science Foundation of China under Grants 61804151, 11774343, 51672264, 61727822, 61874119, 61874117, and 11674314, in part by the Jinan Science and Technology Plan under Grant 2019GXRC041 and in part by the Science and Technology Development Project of Jilin Province under Grants 20180201014GX, 20180201119GX. Corresponding author: YinLi Zhou (e-mail: zhouyinli@ciomp.ac.cn).

**Abstract:** Vertical-cavity surface-emitting lasers that can be controlled to emit hollow laser beam in certain  $LP_{21}$  mode are proposed and fabricated. A circular inverted surface relief with precisely designed diameter and thickness is introduced through theoretical simulation. The fabricated device shows a stable single  $LP_{21}$  mode operation with excellent robustness of mode and power to temperature. Preliminary analysis attribute the excellent performance of the device to the inverted surface relief, leading to hollow near-field spot distribution.

**Index Terms:** Vertical-cavity surface-emitting lasers, hollow laser beam, inverted surface relief.

## 1. Introduction

Semiconducting vertical-cavity surface-emitting lasers (VCSELs) have emerged as attractive low-cost light sources with advantageous properties, such as low power consumption, surface emission and high modulation bandwidth [1]–[3]. Longitudinal single-mode operation is an inherent character of VCSELs due to their extremely short cavity. By contrast, the large transverse dimensions of VCSELs usually induce oscillation with multiple transverse modes. Based on the application requirements, VCSEL operation modes are broadly classified as single fundamental transverse mode (SM) and multiple transverse mode (MM). SM VCSELs are primarily used in atomic clocks, gesture recognition, illumination, and display applications [4], [5]. MM VCSELs are attractive components for optical data transmission, optical illumination, pumping and laser radars [6]–[11].

High-order transverse mode (HM) VCSELs exhibit novel characteristics, which can be used for many important and emerging applications. VCSELs can emit localized hollow laser beam (HLB) in some particular high-order modes. HLB is a laser beam that consists of a dark central region fully

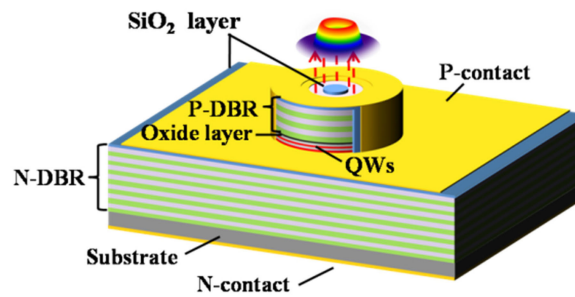


Fig. 1. Three-dimensional sketch of HLB VCSELS.

surrounded by regions of high intensity. The distinct properties of HLB promote its application to the optical-trapping of particles [12], laser-driven ion acceleration [13], and the generation of terahertz radiation [14]. Several general techniques for producing HLB are conical refraction [15], [16], uniaxial crystal [17], interferometer [18], and photon sieve [19]. Most of these techniques require complex and large-scale optical devices. In this letter, we demonstrate a simple VCSEL that can provide HLB from room temperature to high temperature by using an inverted surface relief. With carefully designed diameter and thickness of the inverted surface relief, the device achieves stable HLB emission in single  $LP_{21}$  mode. Compared to traditional techniques for producing HLB, our results provide a monolithic HLB generation method, which greatly simplifies the system complexity.

## 2. Device Design and Fabrication

The epitaxial structure of the VCSEL consists of a cavity placed between n-doped bottom and p-doped top  $Al_{0.12}Ga_{0.88}As/Al_{0.9}Ga_{0.1}As$  distributed Bragg reflector (DBR) built by 34 and 20.5 pairs, respectively. The oxide layer is realized by an 30 nm thickness  $Al_{0.98}Ga_{0.02}As$  layer inserted between the active region and the p-DBR. The oxide aperture was 6  $\mu m$  in diameter. The lasing wavelength of the device is designed to be 895 nm. The schematic drawing of the VCSEL structure is shown in Fig. 1. At the out put window of the VCSEL, 2  $\mu m$  diameter  $SiO_2$  reverse phase layer is deposited at the center of the device to suppress the fundamental transverse mode oscillation.

To design the appropriate  $SiO_2$  reverse phase layer size, mode analysis of the lasing region with 6  $\mu m$  diameter was performed using COMSOL Multiphysics. A model similar to optical fiber is adopted. The material of the core and cladding layer is  $In_{0.1}Ga_{0.9}As$  with refractive index of 3.7603 and  $Al_2O_3$  with refractive index of 1.7578, respectively [20]. The diameter of the core and cladding layer is 6  $\mu m$  and 10  $\mu m$  diameter, respectively. The intensity of some of the lowest-order  $LP_{mn}$  modes that is proportional to the square of the electric field amplitude is shown in Fig. 2. Each mode with  $m \geq 1$  is formed by coupling two identical angular intensity distributions rotated with respect to each other, corresponding to two different polarization states. The  $LP_{01}$  mode is the fundamental transverse mode, and its intensity is confined to the central region of the oxide aperture with a solid round shape. The majority of the intensity of  $LP_{11}$  and  $LP_{21}$  modes is located at the periphery of the oxide aperture with hollow round shapes.

The corresponding 1D distribution of the electric field intensities of  $LP_{01}$ ,  $LP_{11}$ , and  $LP_{21}$  modes is shown in Fig. 3(a). The  $LP_{01}$  and  $LP_{11}$  modes overlap at a certain degrees. To obtain a stable single high-mode operation, the solid round  $SiO_2$  reverse-phase layer is placed at the center of the light-emitting aperture. The radius of the  $SiO_2$  is 1  $\mu m$ , which is equal to the distance between the center of the oxide aperture and the intersection of the  $LP_{01}$  and  $LP_{11}$  modes. The reflectivity of the top DBR with different  $SiO_2$  thicknesses of the VCSEL is calculated by the 1D plane-wave transfer matrix method. The threshold modal gain  $\Gamma g_{th}$  can be expressed as follows [21]:

$$\Gamma g_{th} = \alpha_{in} + \frac{1}{L} \ln \frac{1}{\sqrt{R_t R_d}}$$

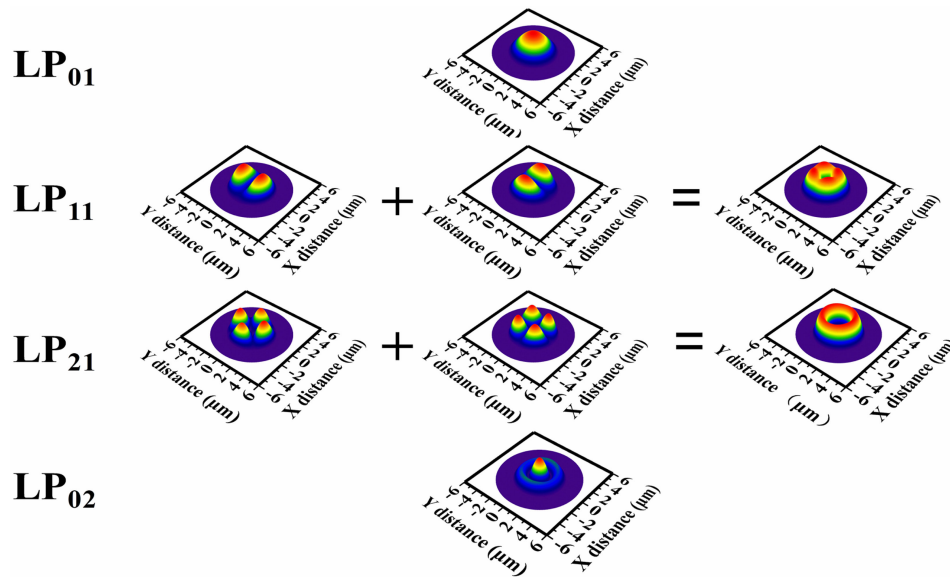


Fig. 2. Calculated distribution of the LP<sub>mn</sub> modes of the VCSEL with 6  $\mu\text{m}$  diameter oxide aperture. The azimuthal number is  $m = 0, 1, 2$ . The radial number is  $n = 1, 2$ .

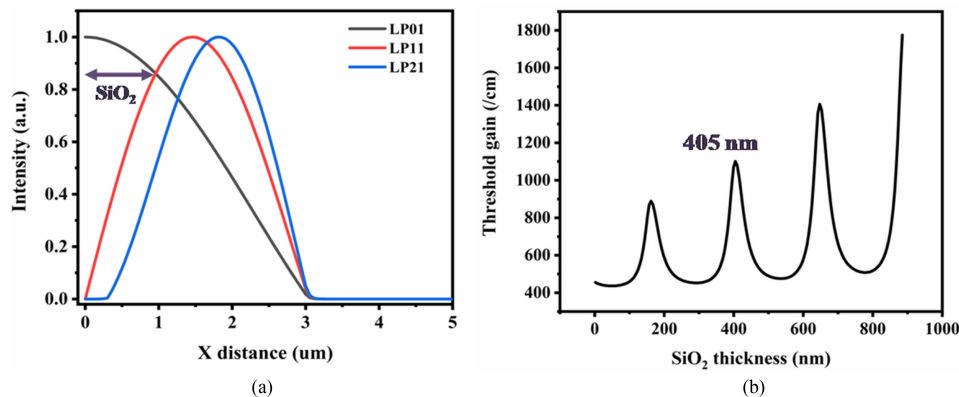


Fig. 3. (a) Distribution of the LP<sub>01</sub>, LP<sub>11</sub>, and LP<sub>21</sub> modes along the radial direction. (b) Relationship between the threshold modal gain and SiO<sub>2</sub> thickness.

where  $\Gamma$  is the optical confinement factor,  $g_{\text{th}}$  is the threshold material gain,  $\alpha_{\text{in}}$  is the intrinsic internal loss,  $R_t$  and  $R_d$  represent the reflectivity of the top and bottom of the DBR, respectively. The relationship between  $\Gamma g_{\text{th}}$  and the thickness of the SiO<sub>2</sub> layer is established in Fig. 3(b). A set of periodic  $\Gamma g_{\text{th}}$  peaks are visible at SiO<sub>2</sub> thickness values equal to the odd times quarter the optical wavelength of SiO<sub>2</sub>. A 405 nm thickness SiO<sub>2</sub> is adopted, in which the LP<sub>01</sub> and LP<sub>11</sub> modes have the maximum threshold modal gain with the highest mirror loss. The lower threshold modal gain of LP<sub>21</sub> mode benefits from the less overlap in space between the SiO<sub>2</sub> reverse-phase layer and the field distribution of the LP<sub>21</sub> mode.

The epitaxial structure of the VCSEL was grown by an AIXTRON 200-4 MOCVD system. The bottom DBR, QW, oxide layer and top DBR layers were deposited on an n-GaAs (001) substrate in order. The VCSEL is fabricated through a standard process. The mesa is formed with inductively coupled plasma reactive ion etching. The oxide aperture with a diameter of 6  $\mu\text{m}$  is formed by

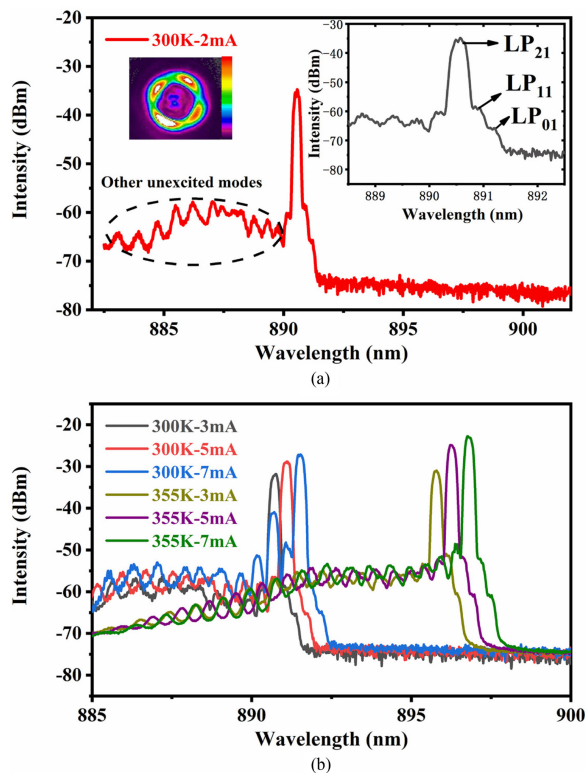


Fig. 4. (a) The measured spectrum and near field of the VCSEL at 300 K and 2 mA, the illustration shows the zoomed details of the same spectrum. (b) Measured spectrum under different currents at 300 K and 355 K.

selectively oxidizing the  $\text{Al}_{0.98}\text{Ga}_{0.02}\text{As}$  layer. Then, the  $\text{SiO}_2$  layer with thickness of 405 nm is deposited by plasma-enhanced chemical vapor deposition. The solid round-shaped  $\text{SiO}_2$  reverse phase layer, electric injection window, and isolation region are defined simultaneously by a single photolithographic process and coupled plasma reaction ion etching. The light-emitting aperture is formed using a lift-off process step.

### 3. Results and Discussion

The spectrum–current characteristic of the VCSEL at different temperatures is shown in Fig. 4. The spectral resolution is 0.02 nm. As displayed in the illustration of Fig. 4(a), the unexcited  $\text{LP}_{01}$  and  $\text{LP}_{11}$  modes are observed, and the  $\text{LP}_{21}$  mode is excited perfectly at 300 K with injection current of 2 mA. The near-field of the  $\text{LP}_{21}$  mode magnified by 100-fold is shown in Fig. 4(a) as a hollow circle with four sidelobes. This result is consistent with the modeling ones shown in Fig. 2. The emergence of the other unexcited modes at shorter wavelengths is due to the large oxide aperture of 6  $\mu\text{m}$ . The spectra that varied with current at 300 K and 355 K are depicted in Fig. 4(b). The device can maintain stable single high-order operation with side-mode suppression ratio (SMSR) greater than 20 dB from 2 mA to 6 mA at 300 K. As the current continues to increase, a higher mode at shorter wavelength appears. A similar scenario does not occur when the current is 9 mA at 355 K. The SMSR of the device rises from 12 dB at 300 K to 26 dB at 355 K when the injection current is 7 mA.

The power–current characteristics of the VCSEL at different temperatures are shown in Fig. 5. The power values with SMSR greater than 20 dB are depicted by solid graphics. Otherwise, the values are represented by a hollow graph. The maximum output power with SMSR greater than 20 dB drops from 3.655 mW (6.2 mA) at 300 K to 2.526 mW (8 mA) at 355 K. The threshold current

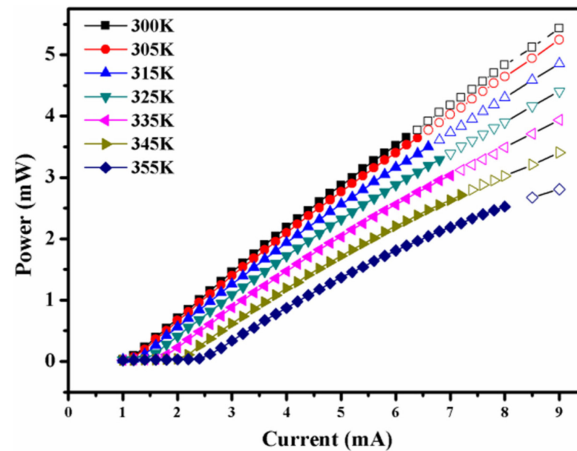


Fig. 5. CW L-I performance of VCSEL at different temperatures.

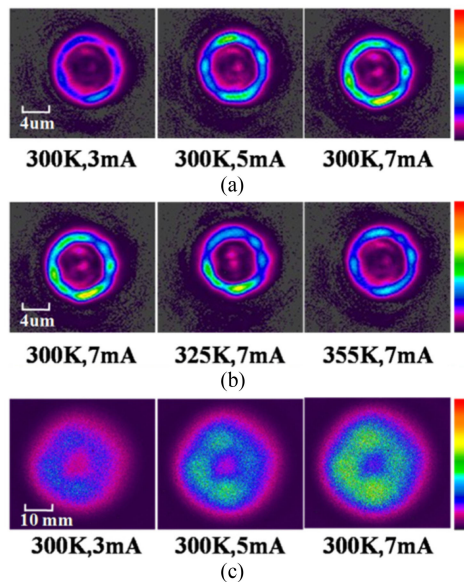


Fig. 6. (a) Measured near-field under different currents at 300 K. (b) Measured near-field under different temperature with injection current of 7 mA. (c) Measured far-field under different currents at 300 K.

of the device increases from 1.06 mA at 300 K to 2.36 mA at 355 K. One important reason for the robustness of mode and power to temperature is the hollow near-field spot distribution of the  $LP_{21}$  mode located in the cooler region compared with that at the center of the active area. The escape of the carriers at the center of the active area is more serious than those at the edge area with temperature increasing. The lower carrier injection efficiency results in a lower gain of the modes that light distributes at the center of the active area. The  $LP_{21}$  mode ultimately oscillates stably at high temperature.

The near fields at different currents and temperatures measured using an eyepiece with a magnification of  $100\times$  are depicted in Figs. 6(a) and (b). To prevent the saturation of the detector, greater attenuation is used when the injection current is greater than 2 mA. A stable hollow circle near-field spot is observed under each test condition. As shown in Fig. 6(a), low-intensity light is observed at the center of the spot when the injection current is higher than 5 mA, which originates

from the unexcited modes. In Fig. 6(b), the decreasing intensity at the center of the spot is attributed to the increase in SMSR at high temperature, which is consistent with the descriptions in Fig. 4. The area of the hollow part of the measured near fields is larger than the simulation results. This phenomenon is due to the fact the measured near fields come from the surface of the device, whereas the simulation results come from the active region, as reported in previous reports [22]. The measured far-field spots under different injection currents at 300 K are shown in Fig. 6(c). A hollow circular spot is always visible with increasing current, which indicates that the device can emit stable HLB.

#### 4. Conclusion

In conclusion, we demonstrate a VCSEL operating at stable single LP<sub>21</sub> mode, which can emit a localized HLB. The maximum single-mode output power of the device is 3.655 mW at 300 K and 2.526 mW at 355 K, with a power drop of only 30.8%. The SMSR of the device at current of 7 mA increases from 12 dB at 300 K to 26 dB at 355 K. The excellent robustness of mode and power to temperature is due to the inverted surface relief, which leads to hollow near-field spot distribution.

#### References

- [1] T. Siegle *et al.*, "Photonic molecules with a tunable inter-cavity gap," *Light Sci. Appl.*, vol. 6, 2017, Art. no. e16224.
- [2] J. W. Zhang, X. Zhang, H. B. Zhu, Y. Q. Ning, L. Qin, and L. J. Wang, "High-temperature operating 894.6 nm-VCSELs with extremely lowthreshold for Cs-based chip scale atomic clocks," *Opt. Express*, vol. 23, no. 11, pp. 14763–14773, 2015.
- [3] Y. Mei *et al.*, "Quantum dot vertical-cavity surface-emitting lasers covering the green gap," *Light Sci. Appl.*, vol. 6, 2017, Art. no. e16199.
- [4] V. Shchukin *et al.*, "Single-mode vertical cavity surface emitting laser via oxide-aperture-engineering of leakage of high-order transverse modes," *IEEE J. Quantum Electron.*, vol. 50, no. 12, pp. 990–995, 2014.
- [5] A. O. Makarov *et al.*, "Investigation of commercial 894.6 nm vertical-cavity surface-emitting lasers for applications in quantum metrology," in *AIP Conf. Proc.*, 2019, Art. no. 2098.
- [6] J. Pozo and E. Beletkaia, "VCSEL technology in the data communication industry," *Photonics Views*, vol. 16, no. 6, pp. 21–23, 2019.
- [7] D. Zhou *et al.*, "Progress on high-power 808 nm VCSELs and applications," *Proc. SPIE*, 10122, 1012206, 2007.
- [8] G. M. Wu, F. C. Kung, and C. Y. Lee, "Study of fabrication and characterization of high power 850 nm vertical-cavity surface-emitting laser arrays," *Surf. Coat. Technol.*, vol. 387, 2020, Art. no. 125489.
- [9] J. W. Zhang *et al.*, "910 nm vertical-cavity surface-emitting laser arrays with 100 W output power level and low driving current," *Jpn. J. Appl. Phys.*, vol. 57, no. 10, 2018, Art. no. 100302.
- [10] C.-T. Tsai *et al.*, "Multi-mode VCSEL chip with high-indium-density InGaAs/AlGaAs quantum-well pairs for QAM-OFDM in multi-mode fiber," *IEEE J. Quantum Electron.*, vol. 53, no. 4, pp. 1–8, 2017.
- [11] K. Szczerba, P. Westbergh, M. Karlsson, P. A. Andrekson, and A. Larsson, "70 Gbps 4-PAM and 56 Gbps 8-PAM using an 850 nm VCSEL," *J. Lightwave Technol.*, vol. 33, no. 7, pp. 1395–1401, 2015.
- [12] Y. L. Pan *et al.*, "Optical-trapping of particles in air using parabolic reflectors and a hollow laser beam," *Opt. Express*, vol. 27, no. 23, pp. 33061–33069, 2019.
- [13] C. Brabetz *et al.*, "Laser-driven ion acceleration with hollow laser beams," *Phys. Plasmas*, vol. 22, no. 1, 2015, Art. no. 013105.
- [14] P. Rawat, V. Rawat, B. Gaur, and G. Purohit, "Generation of terahertz radiation by intense hollow Gaussian laser beam in magnetised plasma under relativistic-ponderomotive regime," *Phys. Plasmas*, vol. 24, no. 7, 2017, Art. no. 073113.
- [15] Y. V. Loiko, A. Turpin, T. K. Kalkandjiev, E. U. Rafailov, and J. Mompert, "Generating a three-dimensional dark focus from a single conically refracted light beam," *Opt. Lett.*, vol. 38, no. 22, pp. 4648–4651, 2013.
- [16] A. Turpin, V. Shvedov, C. Hnatovsky, Y. V. Loiko, and J. Mompert, "Optical vault: A reconfigurable bottle beam based on conical refraction of light," *Opt. Express*, vol. 21, no. 22, pp. 26335–26340, 2013.
- [17] V. G. Shvedov, C. Hnatovsky, N. Shostka, and W. Krolikowski, "Generation of vector bottlebeams with a uniaxial crystal," *J. Opt. Soc. Am. A*, vol. 30, no. 1, pp. 1–6, 2013.
- [18] L. Isenhower, W. Williams, A. Dally, and M. Saffman, "Atom trapping in an interferometrically generated bottle beam trap," *Opt. Lett.*, vol. 34, no. 8, pp. 1159–1161, 2009.
- [19] Y. G. Cheng, J. M. Tong, J. P. Zhu, J. B. Liu, S. Hua, and Y. He, "Clad photon sieve for generating localized hollow beams," *Opt. Laser Eng.*, vol. 77, pp. 7718–7725, 2016.
- [20] M. J. Dodge, "Refractive Index" in *Handbook of Laser Science and Technology*, Volume IV, Optical Materials: Part 2, CRC Press, Boca Raton, 1986, p. 30.
- [21] X. Zhang *et al.*, "894 nm high temperature operating vertical-cavity surface-emitting laser and its application in Cs chip-scale atomic-clock system," *Acta Phys. Sinica*, vol. 65, 2016, Art. no. 134204.
- [22] V. P. Kalosha, N. N. Ledentsov, and D. Bimberg, "Design considerations for large-aperture single-mode oxide-confined vertical-cavity surface-emitting lasers," *Appl. Phys. Lett.*, vol. 101, no. 7, pp. 071117–071120, 2012.